Assessing the Accuracy of Sentinel-2A and the Van Hengel-Spitzer Algorithm for Bathymetry Mapping in Shallow Waters: A Case Study of Bokori Island, Indonesia

Muh Abdul Rahman Hadimu[1], La Ode Muhammad Yasir Haya[1*], Amadhan Takwir[2], Asmadin[2], Muliddin[2] and Asrin Ginong Pratikino[1]

ABSTRACT

Multispectral remote sensing is a proven tool for mapping shallow waters, but accurately capturing seabed color signatures remains a significant challenge due to water- column effects, atmospheric interference, and complex interactions between inherent and apparent optical properties. Our study explores whether Sentinel-2A satellite imagery, processed with the Van Hengel-Spitzer (VHS) algorithm, offers a practical solution for bathymetric mapping. We collected field depth measurements using echo-sounders and adjusted these for tidal variations. Applying the VHS algorithm generated relative depths, which we then calibrated to absolute depths using a linear regression model based on our in-situ data. The results are promising: the combined VHS and Sentinel-2A approach delivered robust depth estimates down to 12 m. The relationship between satellite-derived depths and *in situ* measurements was strong ($R^2 = 0.683$). When we tested accuracy, nearly 80% (79.66%) of the satellite estimates fell within ±3 m of the actual depths. The data also showed higher precision, with 54.24% of estimates accurate within ±2 m and 32.2% within just ±1 m of the measured depths. These findings confirm that Sentinel-2A provides a viable option for moderately accurate, efficient bathymetric mapping in clear, shallow marine environments. This approach holds significant potential for supporting coastal zone management and environmental monitoring efforts.

Keywords: Bathymetry, Indonesia, Remote sensing, Sentinel-2A, Van Hengel-Spitzer algorithm

INTRODUCTION

Currently, accurate mapping of shallow waters is essential for the development of infrastructures in coastal areas and safe navigation around small islands. Unfortunately, in some areas of Eastern Indonesia, shallow-water bathymetric data are still very limited, even though they are needed. Water depth information can provide clues regarding the structure and origin of seabed formations (Chen *et al*., 2018; Janowski *et al*., 2018), provide important information in port terminal construction planning (Šiljeg *et al*., 2019), improve shipping safety (Mavraeidopoulos *et al*., 2017; Hanuransyah *et al.*, 2020), support installation and maintenance of submarine cables and pipelines (Evans and Page, 2014; Setiawan *et al*., 2014; Jung *et al*., 2022), as well as the management of small islands (Agus *et al*., 2021; Kobryn *et al.*, 2022).

Remote sensing technology for shallow water mapping is used to obtain quick, efficient, and effective information about marine phenomena on the surface, in the water column, and at the

[1]Department of Marine Science, Faculty of Fisheries and Marine Science, Halu Oleo University, Kendari, Southeast Sulawesi, Indonesia
[2]Department of Oceanography, Faculty of Mathematics and Natural Sciences, Halu Oleo University, Kendari, Southeast Sulawesi, Indonesia
[*]Corresponding author. E-mail address: laode.haya@uho.ac.id
Received 20 June 2025 / Accepted 10 February 2026

bottom of the waters (Yasir Haya and Fujii, 2017; Lu *et al*., 2021), covering an extensive area (Wu *et al*., 2021; Dematteis *et al*., 2022). Another advantage is that the gathered data may be updated quickly and affordably, making it simple to identify ongoing environmental phenomena (Mahrad *et al*., 2020; Ammirati *et al*., 2022).

One of the challenges in applying remote sensing technology to determine shallow water depth is accuracy. Many studies have examined Satellite-derived bathymetry using medium and high-resolution imagery. Various algorithms have also been widely applied: Setiawan *et al*. (2019) employed the Jupp algorithm on SPOT-7 imagery. Setiawan *et al*. (2014) and Putri *et al*. (2018) used the VHS algorithm on Landsat 8 imagery, Sukmono *et al*. (2022) employed the Lyzenga, Stumpf, and VHS algorithms on Sentinel-2A imagery; and Subarno *et al*. (2015) used the Stumpf algorithm on Sentinel-2A imagery. It is important to note that studies on this topic remain needed in various areas with different characteristics. For example, Su *et al*. (2013) stated that applying certain algorithms for bathymetry determination using multispectral images has not completely overcome bottom-substrate heterogeneity and water turbidity.

This study focuses on assessing the accuracy of the depth values obtained from Sentinel-2A imagery through the application of the VHS algorithm. Using a rotational transformation matrix, Van Hengel and Spitzer (1991) introduced a multispectral reflectance transformation approach. This algorithm also uses visible (multiband) channels in multispectral images. The accuracy test uses simple regression for both single-band and multiband algorithms. Therefore, this study examines the penetration ability at different water depths in each visible band of Sentinel-2A imagery. It also tests accuracy through a combination of regression analysis and bias calculation (i.e., the difference between field depth and the depth based on the VHS algorithm transformation). This accuracy evaluation will aid users in setting tolerance limits for acceptable depth values derived from satellite-based estimates.

MATERIALS AND METHODS

Study area

This study was conducted in the waters around Bokori Island, Konawe Regency, Southeast Sulawesi Province (Figure 1). In addition to its hydro-oceanographic features, the shallow waters around Bokori Island have large seagrass beds, especially in the littoral zone up to six meters deep. The density and types of seagrass vary widely, from sparse to dense areas. Since seagrass reflects less light than light-colored sand, it changes how the seafloor looks in satellite images and can affect depth estimates. These bio-optical traits make this area a good place to test the VHS algorithm across different seafloor types.

Data source

The equipment used for data collection included a MapSounder 585 to collect depth data and a Garmin 64s GPS to assist with navigation. Bathymetric data collection was performed by creating depth-profile (section) measurements. Sounding lines can be perpendicular to the shoreline, concentric lines, or other methods, depending on the method used for determining the bathymetric survey position. In this study, the perpendicular method was used for the bathymetric survey, as it provides detailed depth information (Calder and Mayer, 2003).

The secondary data (tides) used for depth correction were obtained from regulations and reports from relevant agencies/institutions, as well as other references. Additionally, secondary data, in the form of tide data, were obtained from the Kendari Naval Base Headquarters (Markas Komando Lanal Kendari) for Konawe Regency, specifically for 15 days in December 2020.

Sentinel-2A satellite imagery was initially retrieved for May 1, 2020. However, after checking the available images for 2020, the February 2020 scene had the lowest cloud cover and the clearest view. Therefore, imagery acquired in February 2020 was the best for analysis.

Field data collection (sounding) was conducted on December 29, 2020, in the waters around Bokori Island, Konawe Regency, Southeast Sulawesi Province. This is unlikely to affect the analysis because of the temporal mismatch between satellite data and these measurements. We used Sentinel-2A imagery collected in February 2020 for two reasons: (a) shallow-water bathymetric conditions of the study site are stable over time, except when a major geological event (e.g., an underwater earthquake or tsunami) occurs, and (b) images acquired in December 2020 were characterized by reduced water clarity and higher absorption due to rainfall during the rainy season (approximately October–December), which limited their suitability for bathymetric estimation.

Sentinel-2A imagery pre-processing

The imagery pre-processing stage consisted of atmospheric correction using the Dark Object Subtraction (DOS) method (Luca, 2016). Sentinel-2A Level 1C imagery was provided as TOA (Top-of-Atmosphere)reflectance; therefore, it was corrected to BOA (Bottom-of-Atmosphere). BOA correction was performed in QGIS 3.8 using the Semi-Automatic Classification Plugin, producing Sentinel-2A Level 2A imagery (Gatti and Bertolini, 2015). In addition, imagery masking was applied to separate land and sea objects, and during subsequent processing the land reflectance value did not contribute to the marine signal extracted using the VHS algorithm.

Application of the Van Hengel and Spitzer (VHS) algorithm

After the imagery was corrected for atmospheric effects, it was processed using the VHS method. Van Hengel and Spitzer (1991) introduced an algorithm to generate bathymetric information using a rotational transformation matrix of data. This study used the reflectance values from the combination of channels 2, 3, and 4 (visible).

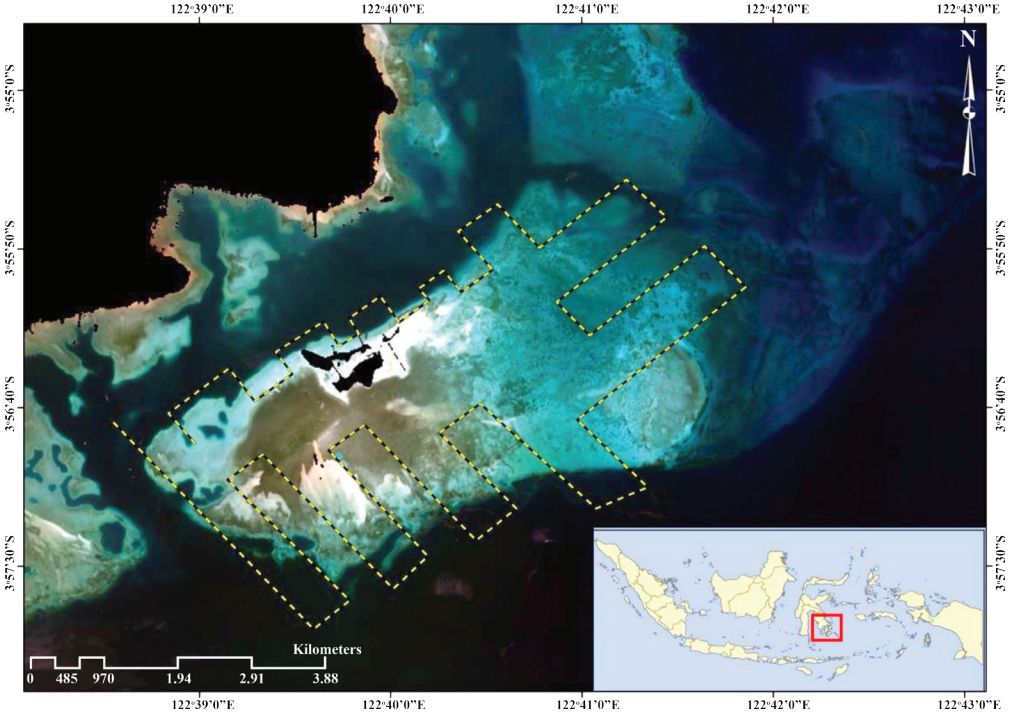


Figure 1. Research location in the waters of Bokori Island, Southeast Sulawesi. The dashed line indicates the echosounder's tracking area.

$$r = \arctan\left(Ur + \sqrt{Ur^2+1}\right)$$

$$s = \arctan\left(Us + \sqrt{Us^2+1}\right)$$

$$Ur = \frac{Var\ x3 + Var\ x2}{2\ Cov\ x2x3}$$

$$Us = \frac{Var\ x4 + Var\ x2}{2\ Cov\ x2x4}$$

where, Var x2 is the variance of channel 2; Var x3 is the variance of channel 3; Var x4 is the variance of channel 4; Cov x2x3 is the covariance of channels 2 and 3; and Cov x2x4 is the covariance of channels 2 and 4.

Ur and Us were computed and used as parameters to calculate r and s. Both r and s were rotation angle values used to calculate the depth index value in the rotational transformation in the VHS algorithm.

$$YI = [\cos(r) \times \sin(s) \times X2] + [\sin(r) \times \cos(s) \times X3] + [\sin(s) \times X4]$$

where, YI is relative depth (Depth Index); and Xi is the reflectance value of channel-i (i = 1, 2, 3, 4).

Regression modeling

Regression analysis was used to determine absolute depth based on the relationship between the relative depth (depth index) and the value of the sounding results in the field. The best model was selected by comparing the fitted equations from the linear, logarithmic, and second-order polynomial regressions.

Accuracy test

A simple linear regression was conducted, and the percentage within each bias tolerance between field depth and imagery-derived dept was calculated to evaluate accuracy level of the absolute depth value. The magnitude of the bias value (difference in depth value) between the field depth and imagery-derived depth was determined using three tolerance levels: ±1, ±2, and ±3 m. The equation used is as follows:

$$bias = \frac{(ni)}{(n)} \times 100\%$$

where, ni is the number of samples in categories ±1, ±2, and ±3 m; and n is the total number of data.

RESULTS AND DISCUSSION

Based on the results, a bathymetric survey carried out in Bokori Island waters provided an overview of water depth, specifically in shallow waters. The sounding results show that the depth ranged between 0.50–25.21 m. The bathymetric data obtained covered all shallow waters along a predetermined sounding path. The reflectance of the Sentinel-2A imagery was matched with the sounding points in the field. The field data served as a reference in determining the depth value using the VHS algorithm. The wavelength composition of the Sentinel-2A satellite used consisted of band 2 or blue (490 nm), 3 or green (560 nm), and 4 or red (665 nm) as can be seen in Figure 2.

According to Figure 2, reflectance varied between the three bands. The reflectance of the red wavelength was lower because it was absorbed more quickly by water. Meanwhile, reflectance was higher in the blue and green wavelengths because the absorption was less. This can be seen from their relatively higher value than the red band, and these values decreased with increasing water depth.

Based on Figure 3, the Green Band (Band 3) showed a stronger relationship than the Blue Band (Band 2). This was also consistent with the weaker performance of the Red Band (Band 4). There were several reasons why this occured, such as: a) penetration and attenuation: in coastal waters, green wavelengths can provide a more useful bottom signal than blue because blue is strongly affected by scattering and water constituents, while red is absorbed quickly; b) signal stability: the green band may be less sensitive than the blue band to atmosphereric and water-column effects (e.g., Rayleigh scattering and suspended/dissolved materials), yielding a more stable relationship with depth; c) substrate suitability, Bokori waters are

dominated by mixed substrates (sand, seagrass, coral). The green band provides a more predictable spectral response to these substrate variations than the blue band; d) effect of atmospheric scattering, although blue has high penetration in very clear water, in satellite imagery, the blue band is most susceptible to atmospheric scattering, which "blurs" the signal from the bottom; e) effect of optically active materials, in tropical waters like Indonesia, the presence of Colored Dissolved Organic Matter (CDOM) and chlorophyll can increase absorption in the blue spectrum, reducing the signal reaching the sensor; f) strong absorption by water, seawater has a very high absorption coefficient for red wavelengths. Red signals barely penetrate more than a few meters, making them less suitable for depth estimation outside the very shallow zone.

In addition, the green channel (band 3) had the best relationship ($R^2 = 0.6427$) compared to the blue and red channels. In theory, channel 2 (blue) has a better ability to penetrate the water column, but it also has the shortest wavelength and is susceptible to atmospheric scattering. Water conditions with a high level of turbidity and a complex substrate mosaic also contributed to uncertainty in depth estimation. Takwir *et al*. (2013) stated that blue channels can penetrate deep waters under several conditions, such as waters with homogeneous substrate conditions, relatively flat seabed topography, and very clear water columns.

Most of the errors in depth estimation using satellite imagery are caused by variations in albedo and reflectance properties of each substrate (Houma *et al*., 2006; Setiawan *et al*., 2019). This implies that the digital values for each channel tend to be inconsistent with the actual depth change. Such conditions can be an obstacle to imagery-based depth accuracy. In addition, bottom-cover types that strongly absorb electromagnetic energy can further reduce the bottom signal, making depth estimation difficult (Jupp, 1988; Green *et al*., 2000; Houma *et al*., 2006; Takwir *et al*., 2013)

The initial stage in processing satellite imagery using the VHS algorithm was to calculate the variance and covariance values shown in Table 2 and Table 3. The next stage was to determine the rotation constants for r and s from the variance and covariance values.

Table 1 presents the variance values used to assess reflectance in each spectral band. Band 3 (green) exhibited the highest variance at 0.00145, indicating the greatest variation across the study

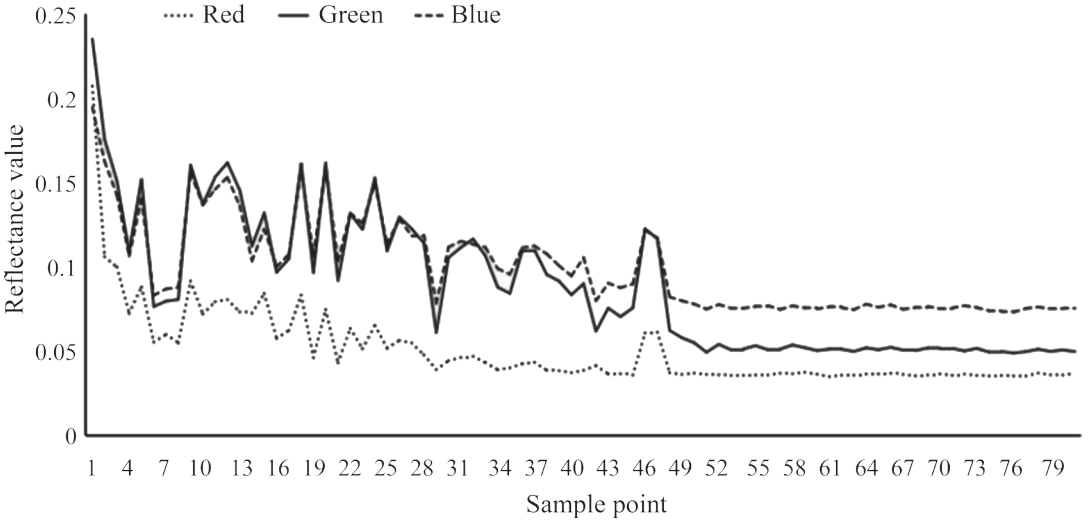


Figure 2. Reflectance values of the Sentinel-2A visible bands (Band 2, blue; Band 3, green; Band 4, red) across the sampled points.

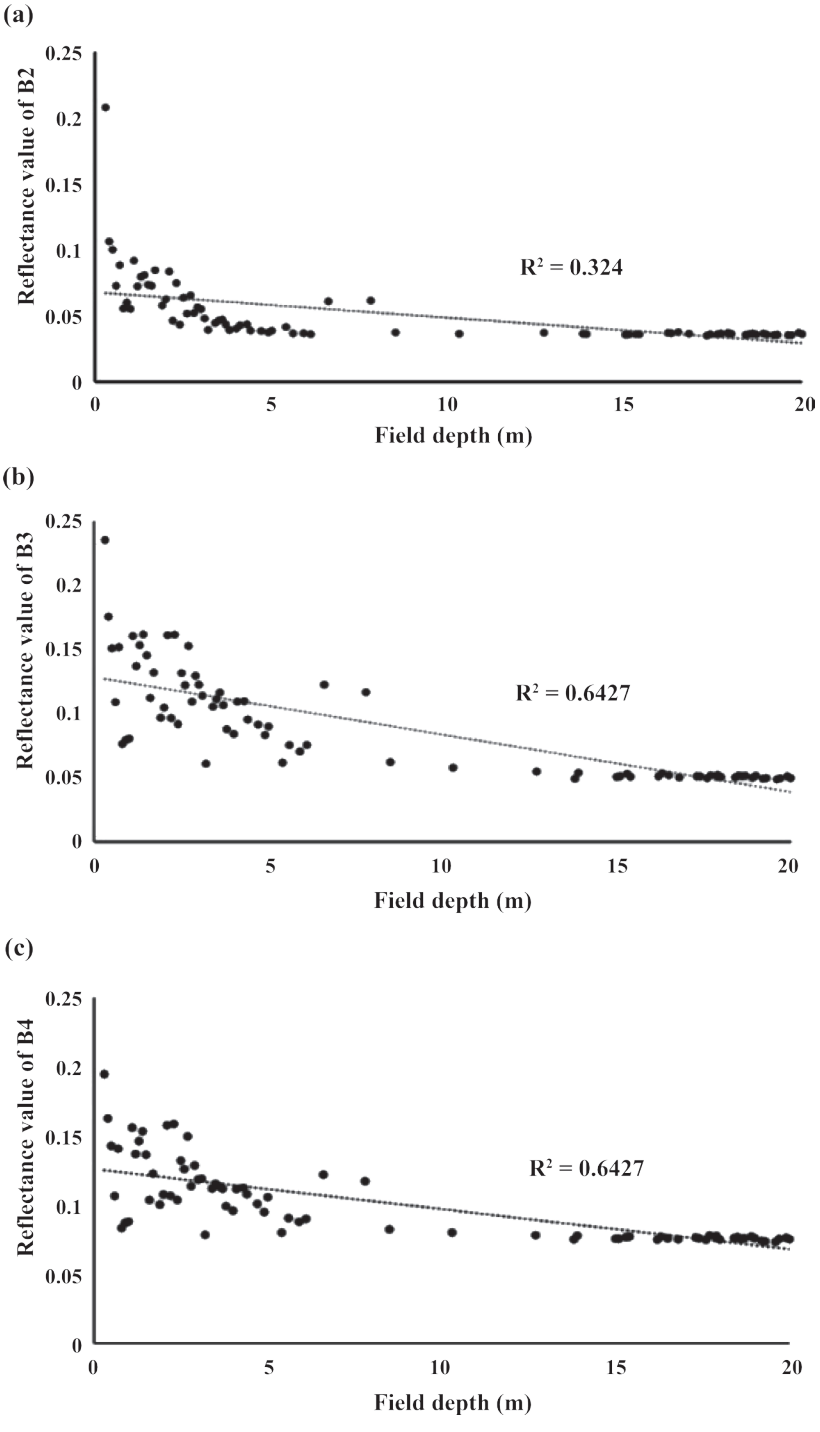


Figure 3. Relationships between tide-corrected in situ (sounding) depth (m) and Sentinel-2A reflectance in (a) Band 2 (blue); (b) Band 3 (green); and (c) Band 4 (red). Dotted lines indicate the fitted regression trends (R^2 shown in each panel).

area and corresponding to its strong association with depth (see Figure 3). In contrast, Band 2 (blue) demonstrated the lowest variance at 0.00048, suggesting more uniform reflectance. This reduced variance may result from atmospheric scattering or specific water conditions.

Table 2 presents the covariance values used to assess the linear relationship between two spectral bands, reflecting shared variation patterns. The highest covariance was observed between Bands 2 and 3 (0.001018898), suggesting that these bands exhibited similar responses to water conditions. These covariance values, together with variance, were utilized to calculate the rotation parameters U_r and U_s in the VHS algorithm, which subsequently was used to generate a depth index.

Tables 1 and 2 show the variance and covariance values for the RGB bands of Sentinel-2A imagery. They were used to calculate the values of U_r and U_s as well as r and s parameters.

Table 3 shows that the rotational parameters r and s are 0.938o and 0.188o, respectively. The values indicate the rotation angles used in the VHS algorithm.

Processing satellite imagery using the VHS algorithm with a 4-3-2 band combination produced a new image expressed in relative YI or depth (depth index). The relative depth (depth index) map can be seen in Figure 4.

Figure 4 illustrates the relative depth estimation results from Sentinel-2A imagery, which represented a depth index that ranges from 0.05 to 0.24. The figure above shows a color gradient, where the darker the water color, the lower the relative depth value. The relative depth value (depth index) from the satellite imagery was not the actual depth; hence, it was processed further to obtain absolute depth estimates based on the selection of the best regression equation.

Table 1. Variance of Sentinel-2A reflectance values for Bands 2 (blue), 3 (green), and 4 (red) used in the VHS algorithm.

Band	Variance value
4	0.00073
3	0.00145
2	0.00048

Table 2. Covariance of Sentinel-2A reflectance values between Band 2 (blue) and Band 3 (green), and between Band 2 (blue) and Band 4 (red), used in the VHS algorithm.

Band	Covariance value
2/3	0.001018898
2/4	0.000488190

Table 3. Rotation parameters (U_r, r, U_s, and s) calculated from Sentinel-2A Bands 4–3–2 (red–green–blue) for the VHS algorithm.

Band combination	Parameter r		Parameter s	
	U_r	r	U_s	s
432	0.947	0.938	0.593	0.188

The pixel value in the relative depth image (YI) was converted into absolute depth to get the actual depth value estimated from the imagery. Therefore, regression analysis was performed on the sounding depth data (*in situ* data) as the X-axis with the relative depth data as the Y-axis. The regression analysis results of the three tested models are as follows.

Regression analysis was used to convert relative depth values to pixel-based estimates of absolute depth (m). Among the tested models, the logarithmic model was selected because it produced the highest R^2 (0.6124), outperforming the linear and second-order polynomial models (Table 4). This choice is also consistent with Setiawan *et al*. (2014). The resulting absolute depth estimates were mapped for easier interpretation; Figure 5 depicts the depth estimation map generated using the VHS algorithm.

The magnitude of the relationship between imagery-derived and field depths was determined by regression analysis using the coefficient of determination (R^2). For the VHS algorithm, the R^2 reflects how well the field (*in situ*) depths explain the estimated absolute depths derived from the reflectance distribution of Sentinel-2A bands. Based on the regression results, the R^2 was 0.683 (Figure 6).

Table 4. Comparison of regression models relating the depth index to *in situ* depth, including the fitted equations and coefficients of determination (R^2).

Regression model	R^2	Equation
Linear	0.5188	y = 0.0054x-0.1369
Logarithmic	0.6124	y = 0.03ln(x)-0.1442
Second- order polynomial	0.584	$y = -0.0005x^2+0.014x-0.1555$

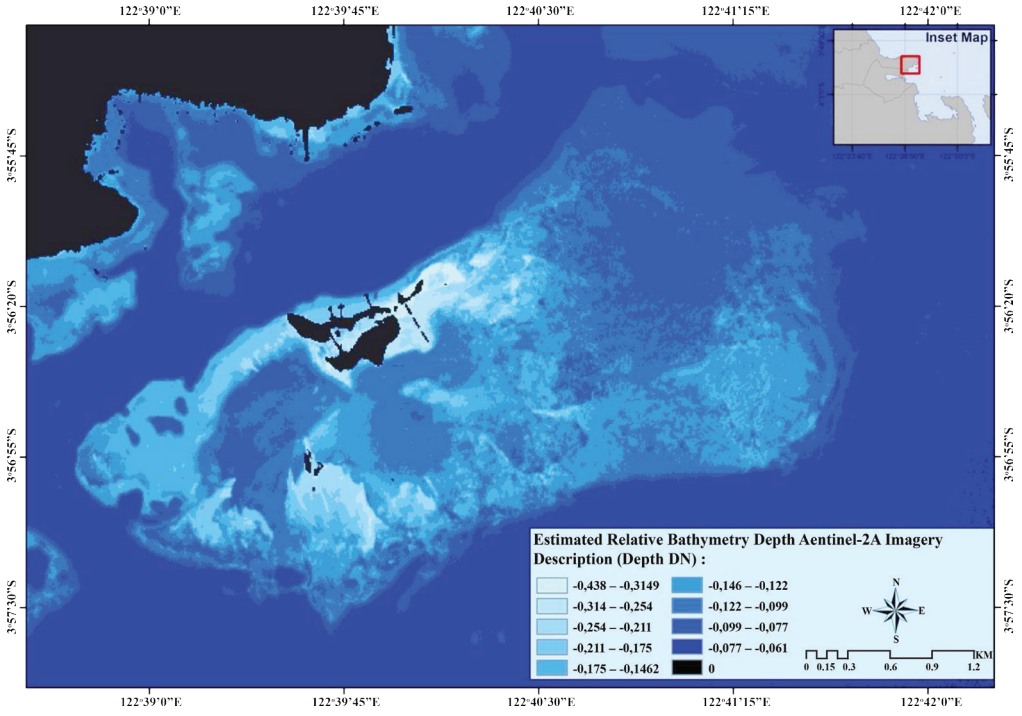


Figure 4. Map of relative depth (depth index, YI) derived from Sentinel-2A imagery using the VHS algorithm. Relative bathymetry classes are shown in color, and the inset indicates the study area location.

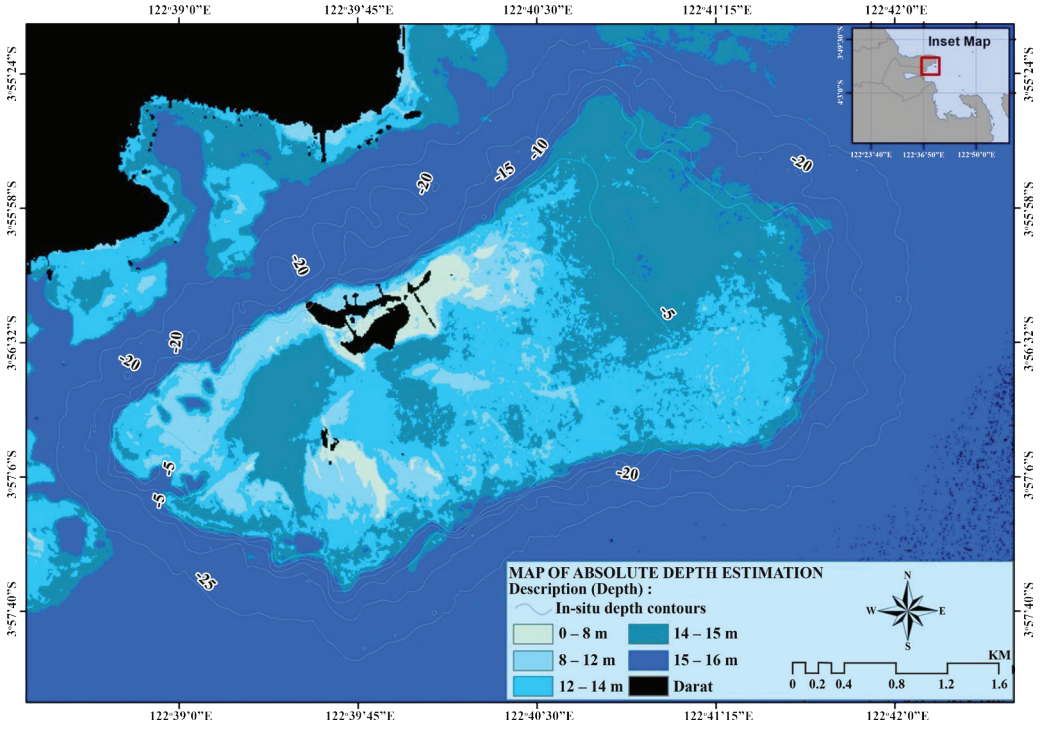


Figure 5. Map of absolute water depth (m) estimated from Sentinel-2A imagery using the VHS algorithm. Depth classes are shown in color, and the *in situ* depth contours are overlaid for comparison; the inset indicates the study area location.

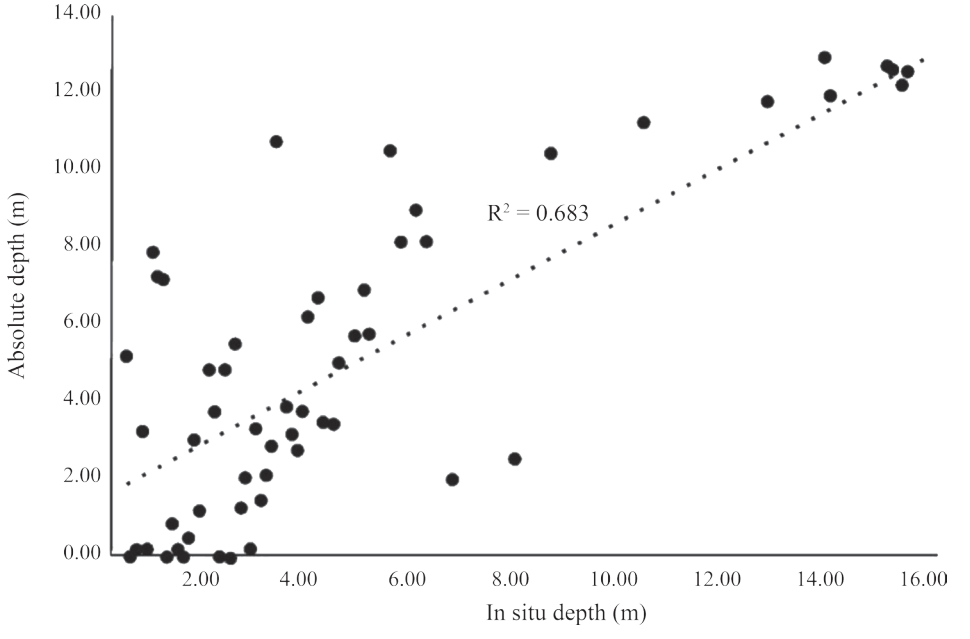


Figure 6. Scatterplot showing the relationship between in situ sounding depth (m) and absolute depth estimated from the VHS algorithm transform (m). The dotted line represents the fitted linear regression ($R^2 = 0.683$).

Errors in absolute depth estimation from Sentinel-2A imagery may result from electromagnetic signal mixing over seagrass bed, as indicated in the 'red box' area in Figure 4 above. This is consistent with Setiawan *et al*. (2019) and Houma *et al*. (2006), who noted that dark substrates such as seagrass are often interpreted as deeper water. In contrast, sandy substrates produce higher reflectance at the same true depth than seagrass substrates.

Depth accuracy was assessed using the bias between the imagery-derived absolute depth and the field depth. Bias tolerance limit of ±1, ±2, ±3, and >3 m were applied to classify accuracy. This approach indicates what proportion of depth estimates is acceptable within each bias limit; conversely, estimates with a bias greater than 2–3 m are considered to have poor accuracy (Figure 7).

The depth accuracy of Sentinel-2A imagery using VHS algorithm at bias tolerances of ±1, ±2, ±3, and >3 m was 32.2%, 54.24%, 79.66%, and 20.34%, respectively. However, the accuracy at the ±1 m tolerance was quite low (Table 5), indicating that this algorithm was not suitable for coastal construction planning that required high-resolution depth information. Nevertheless, it can still be used for preliminary assessments of small-island waters and for conservation activities.

In estimating shallow-water depth using the VHS algorithm, bias (difference) occurs between imagery-derived depth and field depth. This is evident near the coast, where heterogeneous substrates produce different reflectance values. Several factors can cause large bias between field and estimated absolute depth. Subarno *et al*. (2015) reported that bias arose from different spectral responses of different substrates, which can reduce the correlation between digital values and measured depth. Furthermore, Green *et al*. (2020) noted that electromagnetic energy penetrating the water column was partly absorbed and converted into heat or chemical energy for photosynthesis.

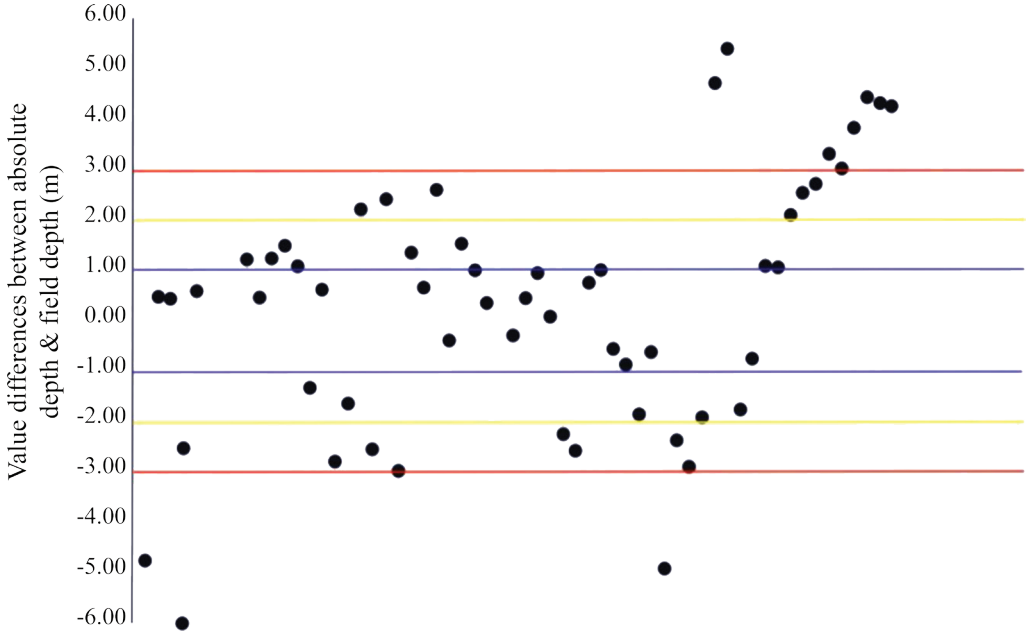


Figure 7. Distribution of bias (field depth-absolute depth, m) between imagery-derived and *in situ* depths. Horizontal reference lines indicateat tolerance limits of ±1 m (blue line), ±2 m (green line), ±3 m (red line), and > 3 m.

Table 5. Accuracy of Sentinel-2A depth estimates using the VHS algorithm, expressed as the percentage of observations within each depth-bias tolerance (±1, ±2, ±3, and >3 m).

Depth bias tolerance (m)	VHS algorithm			
	±1	±2	±3	>3m
Sentinel-2A imagery accuracy (%)	32.2	54.24	79.66	20.34

This study showed that the VHS algorithm could estimate depths up to 12 m, but large bias occured in areas with dense seagrass cover. This differs somewhat from Setiawan *et al*. (2014), who applied the same approach using Landsat 8 imagery and assessed depth up to 5 m around Panggang Island (Seribu Island). In another setting, the VHS algorithm estimated depths up to 22 m ($R^2 = 0.62$) using Landsat ETM+ imagery around Menjangan Island, Bali (Setiawan *et al*., 2014). Putri *et al*. (2018) also reported estimates up to a depth of 30 m using the VHS algorithm on Landsat8 imagery in the very clear waters of Bangsring Beach.

Overall, this study highlights the potential of satellite-based bathymetry as a faster and lower-cost approach for mapping shallow-water areas. These results help can support coastal planning, environmental monitoring, disaster response, and marine resource management (Caballero and Stumpf, 2020; Mokhtar *et al*., 2023), and provide useful information for policymakers, conservation practitioners, and coastal communities.

CONCLUSIONS

Sentinel-2A satellite images processed with the Van Hengel-Spitzer (VHS) algorithm estimated shallow-water depths up to 12 m around Bokori Island, with reasonable accuracy for medium-scale bathymetric mapping. The R^2 value (0.683) indicates a strong relationship between satellite-derived and *in situ* depths. However, performance was lower in some areas. In locations with dense seagrass, depth estimates were often biased because the seafloor's low reflectance caused the spectral model to interpret the water as deeper. Only 32.2% of the estimates fell within ±1 m, indicating that the method is not suitable for applications requiring high precision. In contrast, 79.66% of estimates were within ±3 m, supporting its use for zone-based monitoring, early coastal assessments, and management. This method performed best in clear water over relatively flat seafloors; in areas with seagrass or complex substrates, additional corrections or supplementary data are needed.

ACKNOWLEDGEMENT

We would like to thank Prof Muh Zamrun Firihu (Rector) and Prof La Sara (Dean) for their support.

LITERATURE CITED

Agus, S.B., V.P. Siregar, S.B. Susilo, M.S. Sangadji, G.F. Tasirileleu and P.S. Budi. 2021. Mapping of shallow water bathymetry and reef geomorphology using Sentinel-2 satellite imagery in Genteng Besar and Genteng Kecil Island, Kepulauan Seribu. **IOP Conference Series: Earth and Environmental Science** 944(1): 012048. DOI: 10.1088/1755-1315/944/1/012048.

Ammirati, L., R. Chirico, D. Di Martire and N. Mondillo. 2022. Application of multispectral remote sensing for mapping flood-affected zones in the Brumadinho Mining District (Minas Gerais, Brasil). **Remote Sensing** 14(6): 1501. DOI: 10.3390/rs14061501.

Caballero, I. and R.P. Stumpf. 2020. Towards routine mapping of shallow bathymetry in environments with variable turbidity: Contribution of Sentinel-2A/B satellites mission. **Remote Sensing** 12(3): 1–23. DOI: 10.3390/rs12030451.

Calder, B.R. and L.A. Mayer. 2003. Automatic processing of high-rate, high-density multibeam echosounder data. **Geochemistry, Geophysics, Geosystems** 4(6): 1–22. DOI: 10.1029/2002GC000486.

Chen, J., H. Song, Y. Guan, L.M. Pinheiro and M. Geng. 2018. Geological and oceanographic controls on seabed fluid escape structures in the northern Zhongjiannan Basin, South China Sea. **Journal of Asian Earth Sciences** 168: 38–47. DOI: 10.1016/j.jseaes.2018.04.027.

Dematteis, N., D. Giordan, B. Crippa and O. Monserrat. 2022. Fast local adaptive multiscale image matching algorithm for remote sensing image correlation. **Computers and Geosciences** 159: 104988. DOI: 10.1016/j.cageo.2021.104988.

Evans, G. and M. Page. 2014. **The planning and surveying of submarine cable routes.** In: Submarine Cables. (eds. D.R. Burnett, R. Beckman and T.M. Davenport), pp. 91–122. Brill Nijhoff, Leiden, Netherlands.

Gatti, A. and A. Bertolini. 2015. **Sentinel-2 products specification document.** https://sentinel.esa.int/documents/247904/685211/Sentinel-2-Product-SpecificationsDocument. Cited 13 Jun 2024.

Green, E, P. Mumby, A. Edwards and C. Clark. 2000. **Remote Sensing: Handbook for Tropical Coastal Management.** United Nations Educational, Scientific and Cultural Organization (UNESCO), Place de Fontenoy, Paris, France. 316 pp.

Hanuransyah, M.R., A. Satriadi, K. Kunarso, E.B. Putra and J. Marwoto. 2020. Bathymetry and seabed morphology study for determination of ASDP shipping line in Tanjungsau Island Waters, Batam. **Indonesian Journal of Oceanography** 2(1): 2714–8726. DOI: 10.14710/ijoce.v2i1.7289.

Houma, F., R. Belkessa and N. Bachari. 2006. Contribution of multispectral satellite imagery to the bathymetric analysis of coastal sea bottom. **Revue Des Énergies Renouvelables** 9(3): 165–172.

Janowski, Ł., J. Tęgowski and J. Nowak. 2018. Seafloor mapping based on multibeam echosounder bathymetry and backscatter data using object-based image analysis: a case study from the Rewal site, the Southern Baltic. **Oceanological and Hydrobiological Studies** 47(3): 248–259.

Jung, J., Y. Lee, J. Park and T.K. Yeu. 2022. Multi-modal sonar mapping of offshore cable lines with an autonomous surface vehicle. **Journal of Marine Science and Engineering** 10(3): 361. DOI: 10.3390/jmse10030361.

Jupp, D.L.B. 1988. **Background and extensions to depth of penetration (DOP) mapping in shallow coastal waters.** Proceedings of the Symposium on Remote Sensing of the Coastal Zone Quensland 1988: 91–122.

Kobryn, H.T., L.E. Beckley and K. Wouters. 2022. Bathymetry derivatives and habitat data from hyperspectral imagery establish a high-resolution baseline for managing the Ningaloo Reef, Western Australia. **Remote Sensing** 14(8): 1827. DOI: 10.3390/rs14081827.

Lu, H., Q. Liu, X. Liu and Y. Zhang. 2021. A survey of semantic construction and application of satellite remote sensing images and data. **Journal of Organizational and End User Computing** 33(6): 1–20.

Luca, C. 2016. **From GIS to remote sensing semi automatic classification plugin.** https://fromgistors.blogspot.com/p/semi-automaticclassificationplugin.html. Cited 30 Jan 2022.

Mahrad, B.E., A. Newton, J.D. Icely, I. Kacimi, S. Abalansa and M. Snoussi. 2020. Contribution of remote sensing technologies to a holistic coastal and marine environmental management framework: a review. **Remote Sensing** 12(14): 2313. DOI: 10.3390/rs12142313.

Mavraeidopoulos, A.K., A. Pallikaris and E. Oikonomou. 2017. Satellite derived bathymetry (SDB) and safety of navigation. **The International Hydrographic Review** 17: 7–19.

Mokhtar, K., L.F. Chuah, M.A. Abdullah, O. Oloruntobi, S.M.M. Ruslan, G. Albasher, A. Ali and M.S. Akhtar. 2023. Assessing coastal bathymetry and climate change impacts on coastal ecosystems using Landsat 8 and Sentinel-2 satellite imagery. **Environmental Research** 239: 117314. DOI: 10.1016/j.envres.2023.117314.

Putri, J.C.A., M.A.Z. Fuad and M.A. As'Adi. 2018. Bathymetry mapping using Landsat 8 multyspectral data of Bangsring coastal area. **Omni-Akuatika** 14(1): 54–61.

Setiawan, K.T., T. Osawa and I.W. Nuarsa. 2014. Application of the van hengel and spitzer algorithm for the extraction of bathymetric information using landsat data. **International Journal of Remote Sensing and Earth Sciences** 11(1): 73–80.

Setiawan, K.T., D.B. Ginting, G. Winarso, M.D.M. Manessa, N. Anggraini, A. Julzarika, I. Effendi, S. Rosid and A.H. Supardjo. 2019. May. Development of bathymetry extraction model from SPOT 7 satellite image. **IOP Conference Series: Earth and Environmental Science** 284(1): 012032. DOI: 10.1088/1755-1315/284/1/012032.

Šiljeg, A., B. Cavrić, I. Marić and M. Barada. 2019. GIS modelling of bathymetric data in the construction of port terminals–An example of Vlaška channel in the Port of Ploče, Croatia. **International Journal for Engineering Modelling** 32(1): 17–37. DOI: 10.31534/engmod.2019.1.ri.01m.

Su, H., H. Liu, W. Lei, M. Philipi, W. Heyman and A. Beck. 2013. Geographically adaptive inversion model for improving bathymetric retrieval from multispectral satellite imagery. **IEEE Transaction on Geosciences and Remote Sensing** 52(1): 465–476. DOI: 10.1109/TGRS.2013.2241772.

Subarno, T., V.P. Siregar and S.B. Agus. 2015. Evaluation of Worldview-2 imagery for the estimation of the depth of the shallow waters of Kelapa-Harapan Island using a band ratio algorithm. **Geoplanning: Journal of Geomatics and Planning** 2(1): 30–37.

Sukmono, A., S. Aji, F.J. Amarrohman, N. Bashit and L.R. Saputra. 2022. The Extraction of Near-Shore Bathymetry using Sentinel-2A Satellite Imagery: Algorithms and Their Modifications. **TEM Journal** 11(1): 150–158. DOI: 10.18421/TEM111-17.

Takwir, A., V.P. Siregar and S. Wouthuyzen. 2013. **Validation test of the JUPP algorithm for shallow water bathymetry mapping using alos imagery.** Proceedings of the National Seminar "Strategies for Building a Maritime State" 2013: 136–144.

Van Hengel, W. and D. Spitzer. 1991. Multi-temporal water depth mapping by means of Landsat TM. **International Journal of Remote Sensing** 12(4): 703–712. DOI: 10.1080/01431169108929687.

Wu, T., J. Luo, L. Gao, et al. 2021. Geo-object-based vegetation mapping via machine learning methods with an intelligent sample collection scheme: A case study of Taibai Mountain, China. **Remote Sensing** 13(2): 249. DOI: 10.3390/rs13020249.

Yasir Haya, L.O.M. and M. Fujii. 2017. Mapping the change of coral reefs using remote sensing and in situ measurements: a case study in Pangkajene and Kepulauan Regency, Spermonde Archipelago, Indonesia. **Journal of Oceanography** 73(5): 623–645. DOI: 10.1007/s10872-017-0422-4.